Design and Analysis of Binary Beam Shapers Using Error Diffusion

Introduction

Controlling the amplitude and phase of light is crucial in many technological applications, such as imaging, lithography, astronomy, and laser physics. In high-power laser systems, there is a need for precise beam shaping. Square beams with super-Gaussian profiles are used to optimize the fill factor of amplifiers. The spatially dependent gain of amplifiers can be, to a large extent, precompensated, i.e., the spatial intensity of the beam to be amplified is shaped before amplification so that regions of higher gain in the amplifier correspond to regions of lower intensities in the input beam. To avoid damage or small-scale self-focusing, local intensity variations should be minimized and intensities kept below damaging intensities; therefore, there is a need for accurate beam-shaping systems with fine controls. While spatial light modulator (SLM) technology[1] is well developed, it is not a perfect fit for these applications, since the damage threshold of most SLM's is lower than the required operating fluences for some applications. Because of saturation in laser amplifiers and nonlinear effects such as those encountered in optical parametric chirped-pulse amplification,[2] precompensation may need to be performed at locations in the system where the fluence is already significant (for example, after a first stage of amplification). Beam shaping has been demonstrated using the modal discrimination of a laser cavity or regenerative amplifier cavity (for example, using intracavity phase masks[3,4]), but no elaborate beam-shaping function has been performed beyond the realization of flat-top beams. Additionally, some degree of complexity is added by the realization of a laser cavity combining amplification and shaping, compared to an architecture where these functions are performed by independent elements that can be optimized separately. A large variety of techniques have been demonstrated to generate a spatially varying transmission, such as photographic plates,[5] mirrors with variable reflectivity,[6] elements with spatially varying birefringence,[7] and elements with spatially varying transmission based on total internal reflection.[8] It is unclear, however, if any of these techniques has the required versatility and reliability.

Historically, the solution for shaping high-energy laser beams has been to propagate the beam in a glass substrate with metal patterns on the input surface, where regions coated with metal block the light while clear regions have a 100% transmission. Super-Gaussian beams can, for example, be generated by serrated tooth apodizers,[9] i.e., apodizers with a high-frequency periodic structure where the duty cycle varies as a function of the distance to the center of the plate, which provides a smooth apodization function after Fourier filtering. These apodizers are appropriate for edge-only shaping, i.e., realizing a smooth transition from the high transmission at the center of the beam to the absence of transmission on the edges. However, they cannot generate more-complex shaping functions. Smooth shaping functions can be generated using a vacuum-deposited layer of a metal such as aluminum.[10] More control can be obtained via binary pixelated arrays of metal pixels, as used on the National Ignition Facility[11] to precompensate for the spatial gain variation of large glass amplifiers.[12]

Figure 108.46 displays two examples of target transmission. In Fig. 108.46(a), the target transmission is a 40th-order super-Gaussian that is used in high-power lasers to optimize the fill factor in large-scale slab amplifiers, while decreasing the detrimental effects of diffraction that would occur with a sharp-edge square beam. The corresponding lineout is plotted in Fig. 108.46(c). In Fig. 108.46(b), the target transmission corresponds to the precompensation of the spatially dependent gain of 58 passes in 40-cm-diam Nd:glass disks, as required for OMEGA EP.[13] The corresponding lineout, plotted in Fig. 108.46(d), demonstrates the required nonsymmetric shape due to the uneven distribution of the orientations of the disks. While the apodizing function of Fig. 108.46(a) can be synthesized with serrated tooth apodizers, this approach does not work for the more-complex function of Fig. 108.46(b). Such precompensation is mandatory for large-scale laser systems.[10]

Gray-scale rendering with black or white features is crucial in printing applications, where it is usually referred to as digital half-toning or spatial dithering.[14] Among many other algorithms,[14] the error diffusion algorithm has been identified as particularly efficient at providing gray-scale images with visually pleasing results.[15] Because of the analogy between image

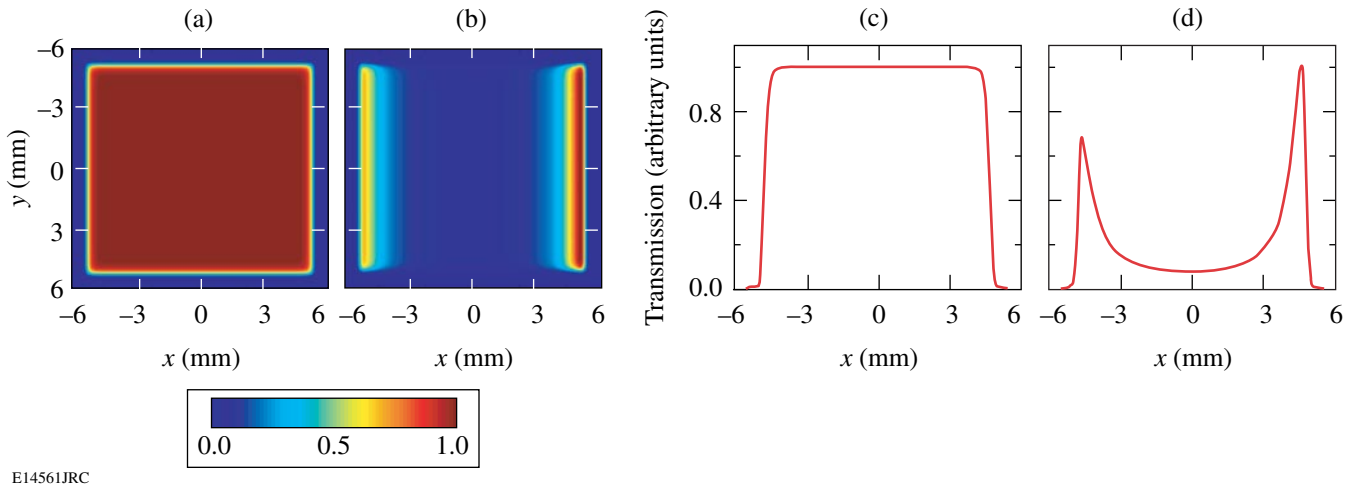

Figure 108.46
(a) Example of 40th-order super-Gaussian intensity; (b) example of intensity distribution required to precompensate for the spatial gain variation in OMEGA EP; (c) lineout of the intensity of (a) at the center of the beam along the x direction; (d) lineout of the intensity of (b) at the center of the beam along the x direction.

rendering and transmission shaping, it is of interest to study the performance of error diffusion when designing binary masks leading to continuous beam-shaping functions. The purpose of this article is to provide insight into the potential and limitations of this technique. The principle of error diffusion and its application to the design of pixelated binary masks are presented first. The performance of the obtained masks in terms of beam shaping is then studied in the context of high-power laser systems. Finally, the influence of feature size on the shaping performance is studied analytically and via simulations.

Error Diffusion Principle

1. Shaping of a Coherent Light Source

It is assumed that a coherent source with constant intensity $I_0 = |E_0|^2$ is incident on a transmission mask, which is relay imaged to the image plane, following Fig. 108.47. A Fourier plane in the imaging system can be used for Fourier filtering. An example of such a system is a two-lens system, with lenses of identical focal length, for which Fourier filtering can be performed with a pinhole at the Fourier plane of the first lens. For the sake of simplicity, we assume an imaging system with magnification equal to 1. The electric field after the binary mask with transmission $s(x,y)$ is $E(x,y) = E_0 \times s(x,y)$, where $s(x,y)$ is either 0 (presence of light-blocking metal) or 1 (no metal) and is pixelated. The electric field at a Fourier plane of the first lens is written as $E_0 \times \tilde{s}(u,v)$, where $\tilde{s}$ is the Fourier transform of s. This field is filtered by a transmission filter p, leading to the field $E_0 \times \tilde{s}(u,v) \times p(u,v)$. The resulting field at an image plane can be written as a convolution $E' = E_0 \times s \otimes \tilde{p}$. Because the convolution with the Fourier transform of the filter $\tilde{p}$ acts as a local averaging operation on the electric field of light after the shaper, the intensity of the output field at a given point (x,y) is proportional to the square of the average value of s around this point. This is important when designing a beam shaper for a spatially coherent light source because the average transmission of the beam shaper before filtering must be designed to be equal to the square root of the target intensity transmission after filtering. The averaging operation provided by the filter in the far field is the key point in obtaining a smooth continuous intensity from a binary pixelated mask.

2. Design of a Binary Beam Shaper Using Error Diffusion

Error diffusion[14,16,17] is based on the lexicographical processing of the pixels of the mask, typically from top to bottom and left to right, following the diagrams in Fig. 108.48.

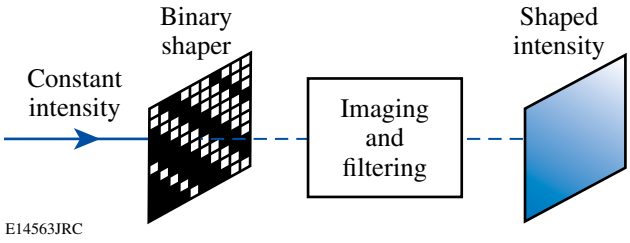

Figure 108.47
Principle of the generation of a continuous shaped intensity using a binary shaper and Fourier filtering.

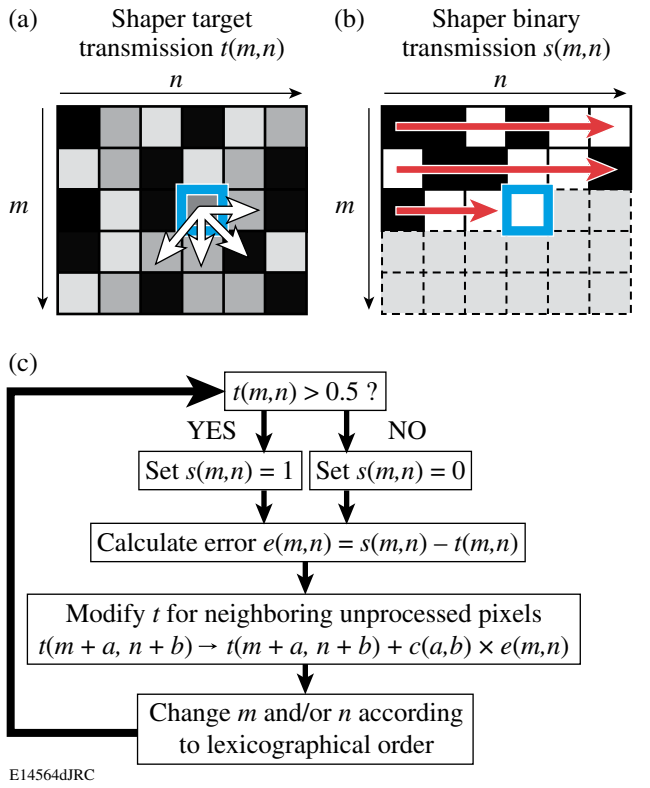

Figure 108.48
Principle of the error diffusion algorithm. (a) Representation of the target shaper transmission $t(m,n)$; (b) representation of the binary shaper transmission $s(m,n)$ being designed; (c) chart describing the design process. The thick squares on (a) and (b) represent the pixel being processed. The horizontal arrows on (b) schematize the lexicographical process over the already processed pixels. The white arrows on (a) represent the error diffusion to adjacent nonprocessed pixels.

A pixelated representation of the target transmission of the shaper, $t(m,n)$, is shown in Fig. 108.48(a), while the binary shaper being designed is shown in Fig. 108.48(b). On the latter, previously processed pixels have a transmission $s(m,n)$ equal to either 0 or 1 and are plotted in black or white, while nonprocessed pixels have been arbitrarily plotted in gray. Since the target transmission takes values in the interval [0,1] while the shaper transmission is either 0 or 1, the choice of the value of each pixel in the binary mask induces a transmission error. In error diffusion, the binary value of the pixel (m,n) is set by the information contained in the target shaper transmission $t(m,n)$, which can be modified by the choices that have been made for the mask binary value $s(m,n)$ for the pixels that have already been processed. Initially, one sets $t(m,n) = \sqrt{I(m,n)}$, where I is the sampled representation of the target intensity of the coherent source. Following the chart in Fig. 108.48(c), the choice of transmission $s(m,n)$ is made by comparing the target shaper transmission to 0.5. If the target transmission is smaller than 0.5, $s(m,n)$ is set to 0, while, if the transmission is larger than 0.5, $s(m,n)$ is set to 1. The resulting error is "diffused" to pixels that have not yet been processed, usually neighboring pixels, to bias the binary choice for these pixels and locally compensate the transmission error. This is done by adding a fraction of the error $e(m,n) = s(m,n) - t(m,n)$ to the target transmission for these pixels, which is symbolized in Fig. 108.48(a) by white arrows pointing to these pixels. The target transmission $t(m + a, n + b)$ is then replaced by $t(m + a, n + b) + c(a,b) \times e(m,n)$ for the chosen set of integers a and b. In the initial developments of error diffusion by Floyd and Steinberg,[16] only the four neighboring pixels at coordinates $(m + 1, n - 1)$, $(m + 1, n)$, $(m + 1, n + 1)$, and $(m, n + 1)$ are used in the diffusion process (four-weights error diffusion). The results presented in this article have been obtained with such implementation, as the gain of performance when diffusing the error to a large number of neighboring pixels does not seem significant. The function c takes for value $c(1,-1) = -3/16$, $c(1,0) = -5/16$, $c(1,1) = -1/16$, and $c(0,1) = -7/16$. The algorithm then proceeds with the next pixel, following the lexicographical order.

Properties of Binary Shapers Generated with Error Diffusion

1. Error Functions for Beam-Shaping Performance

Two functions have been used to quantify beam-shaping performance. A normalized version of the rms error between the target shaped intensity and the obtained shaped intensity after filtering is

$$\varepsilon_{\text{rms}} = \sqrt{\iint_S \left[T_{\text{obtained}}(x,y)/T_{\text{target}}(x,y) - 1\right]^2 dxdy}, \quad (1)$$

where the double integral is calculated over the region S, where the target intensity is higher than a given threshold to ensure that only relevant values are kept. The normalization ensures that the calculated error remains the same after multiplication of the target and obtained intensities by a spatially varying function. This ensures that this rms error is also a proper description of the shaping performance after amplification of the shaped beam.

Another error function of interest when dealing with shaping elements for laser applications describes the presence of local high values of the intensity because of the potential damage to optics and self-focusing,

$$\varepsilon_{\text{peak}} = \max_s \left[\frac{T_{\text{obtained}}(x,y)}{T_{\text{target}}(x,y)} - 1\right], \quad (2)$$

where the maximum is calculated over a region of interest (typically, the region where the beam is amplified to signifi-

cant values). This error function quantifies the magnitude of hot spots in the beam. While these two error functions are, in general, not correlated, it was found that they had similar behaviors when varying the pixel size or the parameters of the far-field filtering operation, and we therefore plot only the rms error, but quote the peak error in relevant cases.

2. Comparison of the Error Diffusion Algorithm with the Random Dither Algorithm

A simple random dither algorithm is used to emphasize the properties of the error diffusion algorithm. The random dither algorithm is one of the simplest algorithms that can be used to design binary shaping elements. It is also known as white-noise dithering because of the spectral content of the generated images.[14] While this technique has shortcomings, its simplicity makes it an ideal choice to highlight the properties and performance of the error diffusion algorithm. For the random dither algorithm, the binary transmission of each pixel is chosen by a random draw between 0 and 1. If the drawn number is smaller than the target transmission, the transmission of the pixel is set to 1, while if the drawn number is higher than the target transmission, the transmission of the pixel is set to 0. Properties of random draws ensure that this algorithm properly reproduces gray levels on average. One should note that there is no error feedback in such an algorithm.

3. Properties of the Error Diffusion Algorithm

Pixelated binary masks generated with error diffusion are highly ordered structures. Figure 108.49 displays pixelated binary distributions generated by error diffusion for target transmissions equal to 5%, 25%, and 75%. It was found that the error diffusion algorithm can reproduce gray levels very accurately. These close-ups are compared to close-ups of masks generated by the random dither algorithm to generate the same target transmission. The latter show no correlation between the presence of pixels at various locations in the mask.

To understand the binarization noise, the error diffusion and random dither algorithm were used to generate a shaping function corresponding to Fig. 108.46(b), using 10-μm pixels. The corresponding binary shaper generated by error diffusion is plotted in Fig. 108.50(a), and close-ups of the binary pixel distributions at the center and at the upper right corner are displayed in Figs. 108.50(b) and 108.50(c). A lineout of the shaped intensity plotted in Fig. 108.50(d) demonstrates the proper realization of the transmission of the shaper, including the proper transmission at the center of the beam and the high-frequency content on the edges of the beam, owing to the high resolution and proper rendition of gray levels when using error diffusion.

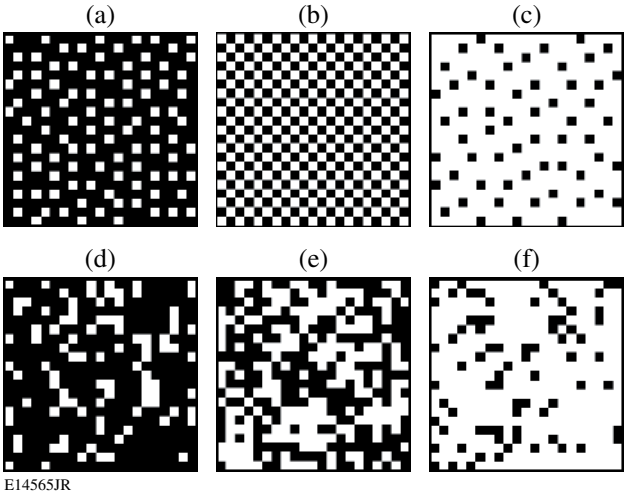

Figure 108.49
(a)–(c) Close-ups of shapers designed with error diffusion for a target-intensity transmission equal to 5%, 25%, and 75%, respectively; (d)–(f) close-ups of shapers designed with the random dither algorithm for a target-intensity transmission equal to 5%, 25%, and 75%, respectively.

This lineout corresponds to the optimal filtering in the Fourier plane, as discussed below. As can be seen, the shaped intensity varies by less than 1% around the target intensity. Intensities of the far field of the shapers generated by error diffusion and random dither are compared in Fig. 108.51, where the average of the far-field intensity in a 4-mrad interval along the y direction has been plotted on a logarithmic scale as a function of the angle in the x direction. The noise due to the binarization is pushed to high frequencies in the case of the error diffusion algorithm but is present at all frequencies in the case of the random dither algorithm—an example of the general behavior of spatially dithered masks generated with error diffusion.[17] The spectrum of the noise introduced by the binarization has no zero-frequency component and has only significant density at high frequencies, therefore the name "blue-noise dithering."[18] By comparison, the randomness of the random draw design algorithm generates a constant noise background in the far field (i.e., "white noise"). This point is particularly important for Fourier filtering because the amplitude filter in the far field (e.g., the pinhole) can effectively block the binarization noise while preserving the frequency content of the target transmission.

To demonstrate the influence of the filtering operation, the rms error is calculated as a function of the angular diameter of a circular pinhole set in the far field for a shaping element designed with error diffusion and random dither to approximate the target-shaped intensity of Fig. 108.46(b). The rms error is also calculated when propagating a field having the

target-shaped intensity. Figure 108.52(a) shows that the rms error is limited at low pinhole sizes by the propagation of the target-shaped intensity through the filtering system (i.e., the high frequencies of this intensity are blocked by the pinhole) that also constrains the rms error in the case of the binary distributions. The error increases quickly for the random dither algorithm as the pinhole size is increased, but decreases in the case of error diffusion. The rms error reaches a minimum for a given pinhole diameter for each design algorithm. The rms error is minimal for a 7-mrad pinhole in the case of error diffusion ($\varepsilon_{rms} = 0.7\%$, $\varepsilon_{peak} = 2.4\%$) and for a 3-mrad pinhole in the case of the random dither algorithm ($\varepsilon_{rms} = 7.5\%$, $\varepsilon_{peak} = 27.4\%$). The corresponding shaped intensities were used to calculate the intensity after amplification, which is expected to be functionally similar to that of Fig. 108.46(a). The three lineouts of the amplified intensity plotted in Figs. 108.53(a)

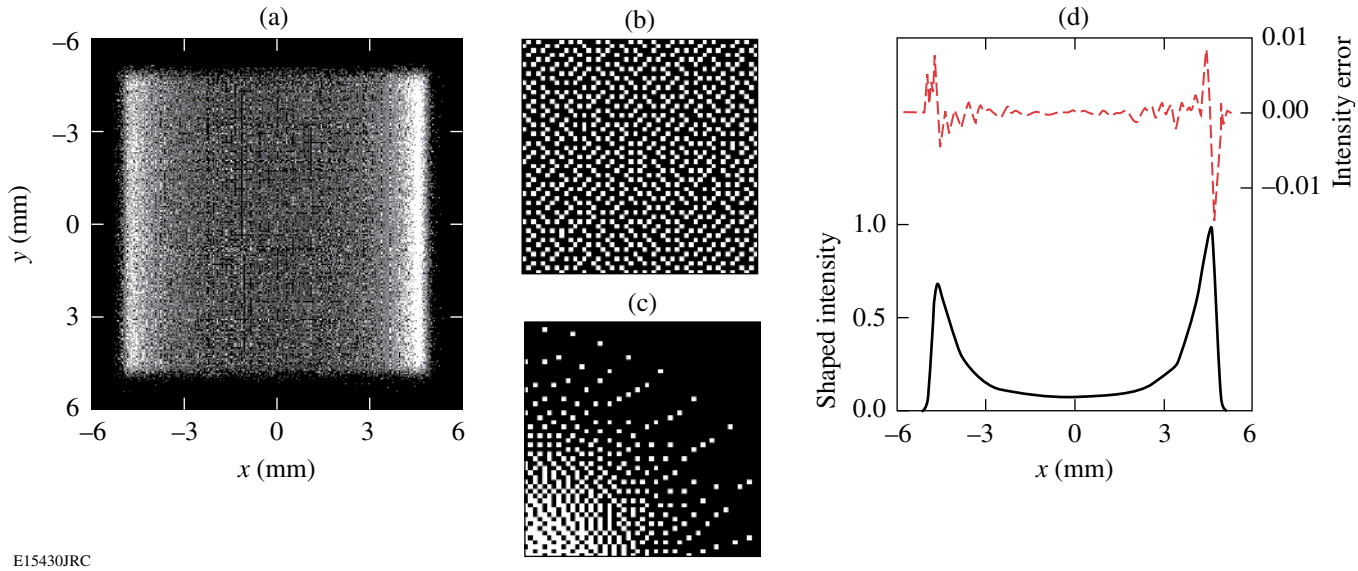

Figure 108.50
(a) Binary shaper corresponding to the transmission of Fig. 108.46(b); (b) and (c): close-ups of the binary pixel distribution at the center and at the upper right corner of the beam, respectively; (d) lineout of the filtered intensity along the x direction (solid line) and lineout of the difference between the filtered intensity and the target intensity (dashed line).

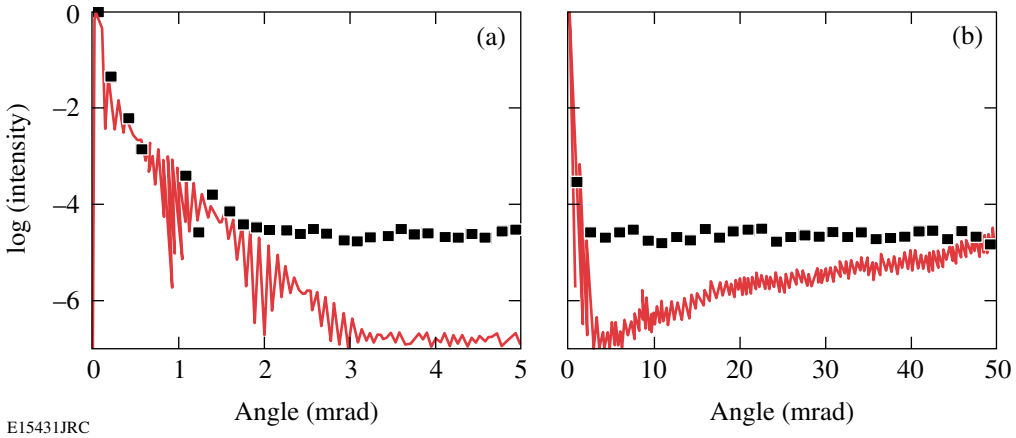

Figure 108.51
Intensity of the far field of the binary beam shaper designed with the error diffusion algorithm (solid line) and the random dither algorithm (squares) for the generation of a shaped intensity of Fig. 108.46(c). The intensity is averaged over a 4-mrad angle in the y direction and plotted versus the angle in the x direction. Plots (a) and (b) cover different ranges of angles.

and 108.53(b) show that the modulations due to the shaping process are not detectable for error diffusion, but are significant for random dither.

We have also studied the effect of pixel size in the design of shapers. It is intuitive that smaller pixels lead to better resolution in the reproduction of the shaping function. This is demonstrated by plotting the rms error as a function of the pinhole diameter for the shaping function of Fig. 108.46(b) designed with error diffusion and binary shapers with 10-, 20-, and 40-μm pixels [Fig. 108.52(b)]. Larger pixels increase the rms error, and influence the shaping performance in two ways: they generally decrease the ability to generate quickly varying functions and, in the case of a binary distribution, they imply a reduction in the number of parameters available to locally specify a gray level (for example, an area of 10-μm binary pixels has 16 times more bits of information than the same area covered with 40-μm pixels). The minimal rms error for a given pixel size is obtained for a pinhole size that decreases when the pixel size is increased. A shaper with 10-μm pixels

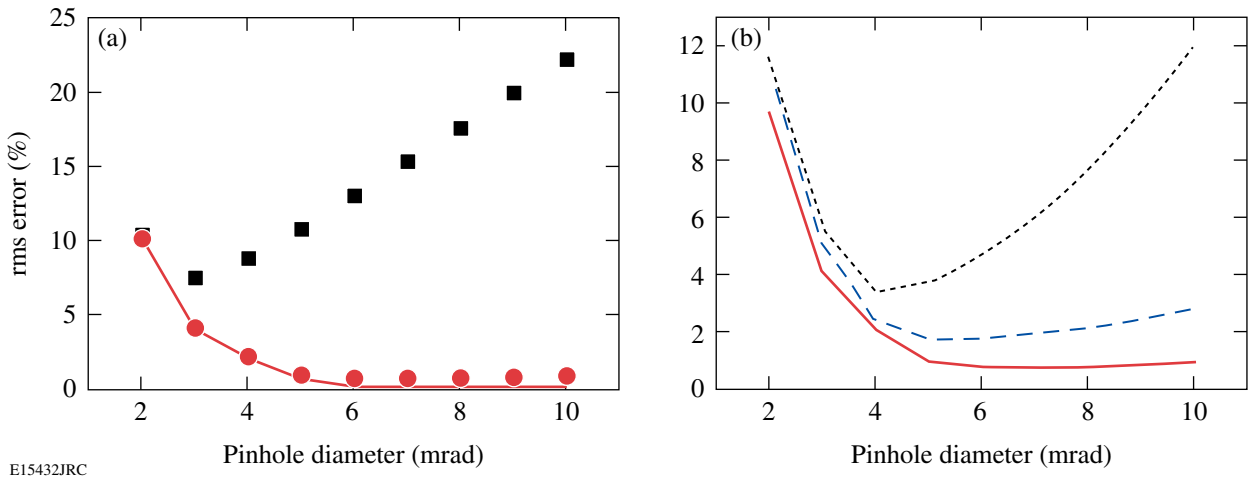

Figure 108.52
(a) rms error for the realization of the shaped intensity of Fig. 108.46(b) as a function of the pinhole angular diameter in the case of the error diffusion algorithm (circles) and the random draw algorithm (squares). The solid line corresponds to the propagation of a field having the target-shaped intensity through the same filtering system. (b) rms error for the realization of the shaped intensity of Fig. 108.46(b) as a function of the pinhole angular diameter for a pixel size of 10 μm (solid line), 20 μm (dashed line), and 40 μm (dotted line) in the case of error diffusion.

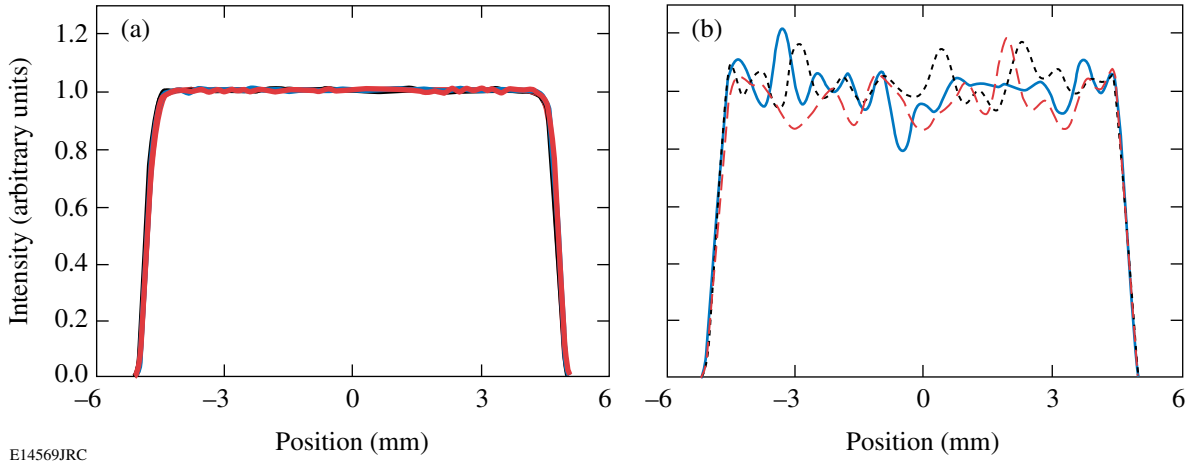

Figure 108.53
Three lineouts of the simulated intensity of the shaped beam after amplification for shaping with (a) error diffusion and (b) random dither. In each case, the pixel size is 10 μm, and the pinhole size leading to the smallest rms error is used.

leads to $\varepsilon_{rms} = 0.7\%$ and $\varepsilon_{peak} = 2.4\%$ with a 7-mrad pinhole; with 20-μm pixels leads to $\varepsilon_{rms} = 1.7\%$ and $\varepsilon_{peak} = 4.3\%$ with a 5-mrad pinhole; and with 40-μm pixels leads to $\varepsilon_{rms} = 3.4\%$ and $\varepsilon_{peak} = 9\%$ with a 4-mrad pinhole.

Effect of Feature-Size Variation on the Shaping Performance

Practical applications of shapers are constrained by the ability to faithfully reproduce small-scale features. A typical process for generating metal masks is based on lithography.[19] In the case of wet-etch lithography, etching can lead to a reduction in feature size, i.e., the light-blocking metal pixels are smaller than specified in the design, which leads to an increased transmission. It is important to understand the scaling of this effect, quantify it, and potentially come up with precompensation schemes.

1. Analytical Derivation

The design of shapers using error diffusion leads to highly ordered distributions of pixels, as shown in the previous section. It has been observed that shapers with isolated 100% transmission blanks [example in Fig. 108.49(a)] were obtained for target transmission smaller than 10%. Shapers with isolated 0% transmission pixels were obtained for target transmissions higher than 45% [example in Fig. 108.49(c)]. In these cases, the transmission can be predicted uniquely from the knowledge of the area of a blank (in the first case) and the area of a pixel (in the second case), these areas being scaled to the expected nominal area for these features.

In the case of isolated blanks, the intensity transmission after Fourier filtering is

$$T_{obtained} = d_{blank}^2 = \left(\frac{B \times S_{blank}}{N \times S_0}\right)^2, \tag{3}$$

where d_{blank} is the density of blank pixels, B is the number of blank pixels in a representative area with a total number of pixels equal to N, S_{blank} is the surface of a blank pixel, and S_0 is the nominal surface of a pixel. Using the fact that $T_{target} = (B/N)^2$, one obtains the relation describing the transmission of regions with isolated blanks as

$$T_{obtained} = T_{target} \times \left(\frac{S_{blank}}{S_0}\right)^2. \tag{4}$$

In the case of isolated pixels, the intensity transmission after Fourier filtering is

$$T_{obtained} = (1 - d_{metal})^2 = \left(1 - \frac{M \times S_{metal}}{N \times S_0}\right)^2, \tag{5}$$

where d_{metal} is the density of metal pixels, M is the number of metal pixels in a representative area with a total number of pixels equal to N, S_{metal} is the surface of a metal pixel, and S_0 is the surface of a pixel. Using the relation $T_{target} = \left[1 - (M/N)\right]^2$, one obtains

$$T_{obtained} = \left[\left(1 - \sqrt{T_{target}}\right) \times \frac{S_{metal}}{S_0} - 1\right]^2. \tag{6}$$

For transmissions between 10% and 45%, analytical derivation is not as simple. In the special case of a target transmission equal to 25%, the generated distribution of pixels is a checkerboard of metal and blank pixels [example in Fig. 108.49(b)], for which it can be seen that the transmission error can be predicted considering isolated metal pixels if the feature-size variation is due to the edge effect simulated below, i.e., using Eq. (6).

2. Simulations

A simulation was performed to quantify the impact of pixel-size mismatch on the transmission of shapers. It is assumed that the primary effect of pixel-size variation is an edge effect, i.e., a metal pixel neighboring a blank pixel is over-etched and an additional section of metal is removed from the corresponding edge. The offset is defined as the ratio of the length of metal additionally removed over the nominal size of the pixel (e.g., nominal 10-μm metal pixels losing 0.5 μm on each side correspond to a 5% offset, and an isolated metal pixel becomes a 9-μm pixel). A mask for a constant transmission T_{target} after filtering is first generated. The edge effect is simulated by increasing the transmission of every blank in the mask by n times the relative change due to the over-etching, where n corresponds to the number of neighboring metal pixels. The obtained transmission is obtained by calculating the actual transmission of the mask after this operation to get $T_{obtained}$. The transmission error is then defined as $\left(T_{obtained}/T_{target}\right) - 1$. While these simulations assume a specific process for the transmission degradation, it has been found to describe accurately our experimental results. One should note however that the formulas of Eq. (4) and Eq. (6) are valid for shapers with isolated blanks and pixels of arbitrary shape.

The transmission error is plotted in Fig. 108.54 as a function of the target transmission in the case of a 5% offset (e.g., 9-μm pixels obtained on a 10-μm grid) and a 10% offset (e.g., 8-μm pixels obtained on a 10-μm grid), with the corresponding analytical prediction calculated using the size of both the metal and blank pixels. The simulations and the analytical predictions of Eq. (4) and Eq. (6) agree well in their respective domain of validity. For over-etched metal pixels, the maximal transmission error is obtained for low target-intensity transmission smaller than 10%. The predicted transmission error at low

design transmission using the surface of a blank and Eq. (4) is, respectively, 44% and 96% for size offset equal to 5% and 10%. This error can be reduced by decreasing the offset in pixel size. While small pixels lead theoretically to better shaping capabilities, the absolute reduction in metal pixel size due to lithography is mostly independent of the pixel size, i.e., the offset becomes larger when using smaller pixels. For example, a process leading to a 10% offset error on 10-μm pixels would give only a 5% offset on 20-μm pixels. There is a trade-off between shaping capabilities and transmission error, unless some precompensation of the shaper design taking into account the feature size of the mask is performed.

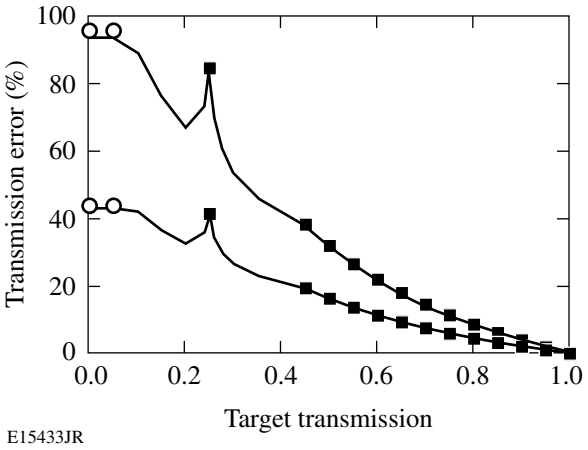

Figure 108.54
Transmission error simulated as a function of the target-intensity transmission for a pixel-size offset equal to 5% (lower curve) and 10% (upper curve). In each case, the circles correspond to the error prediction using Eq. (4) and the squares correspond to the error prediction using Eq. (6) (markers are plotted only in the domain of validity of these two equations).

3. Precompensation

Precompensation of the transmission error due to the feature size is made possible by the predictability of the transmission error. While an exact knowledge of the transmission error requires an exact knowledge of the feature sizes and shapes, one can rely on an approximate model of the pixel shape and size to precompensate the transmission by modifying the pixel density. One starts with the knowledge of the relation between design transmission and obtained transmission, written as $T_{\text{obtained}} = f(T_{\text{design}})$. It suffices to chose $T_{\text{design}} = f^{-1}(T_{\text{target}})$ to obtain $T_{\text{obtained}} = T_{\text{target}}$, where f^{-1} is the reciprocal function of f. Precompensation can be performed simply by applying the error diffusion algorithm to $f^{-1}[T_{\text{target}}(x,y)]$ instead of $T_{\text{target}}(x,y)$. In practice, the exact shape of the function f (and f^{-1}) is not known. It depends on the feature size of the generated shaper as well as the feature shape. These properties are likely to be similar for different runs of the same fabrication process, which allows some precompensation of these effects at the design stage.

The function f calculated in the previous subsection for a 5% offset was used to precompensate the shaper design. As in the previous subsection, shapers with a target transmission ranging from 0% to 100% were generated by applying the error diffusion algorithm. The transmission obtained with these shapers was then calculated, following the previous procedure, for pixels corresponding to offsets equal to 4%, 5%, and 6%. The transmission error in the absence of precompensation for these three offsets is plotted in Fig. 108.55(a). It can be compared to the transmission error with precompensation of a 5% offset, which is plotted in Fig. 108.55(b). A significant reduction of the transmission error is obtained. As expected, the transmission error after precompensation is positive for an offset equal to 6%, approximately equal to zero for an offset of 5%, and negative for an offset equal to 4%.

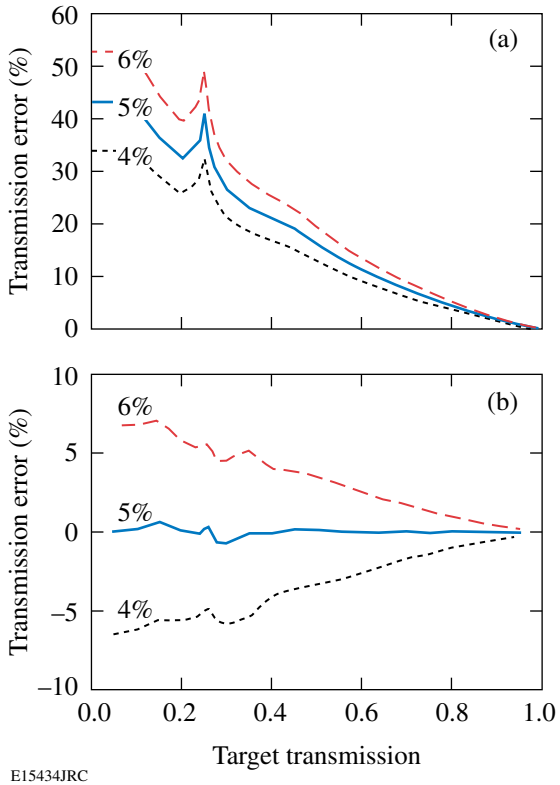

Figure 108.55
Transmission error as a function of the target transmission for pixel-size offsets equal to 4% (dotted line), 5% (solid line), and 6% (dashed line) (a) without precompensation and (b) with precompensation of the pixel-size offset assuming a pixel-size offset equal to 5%.

Conclusion

The error diffusion algorithm has been studied in the context of the design of beam shapers for high-power laser applications. The high resolution and accurate reproduction of continuous shaping functions is beneficial to these applications. In particular, it has been shown that the shaped intensity has no significant hot spots, therefore decreasing the risk of damage in the laser system. The practical problem of accurate feature size reproduction has been studied in detail, and it has been shown that the transmission error can be reduced significantly by proper biasing of the target transmission before applying the design algorithm. The pixel size should be chosen by considering both the theoretical shaping capability and the influence of the practical fabrication process.

ACKNOWLEDGMENT

This work was supported by the U.S. Department of Energy Office of Inertial Confinement Fusion under Cooperative Agreement No. DE-FC52-92SF19460, the University of Rochester, and the New York State Energy Research and Development Authority. The support of DOE does not constitute an endorsement by DOE of the views expressed in this article.

REFERENCES

1. U. Efron, *Spatial Light Modulator Technology: Materials, Devices, and Applications*, Optical Engineering, Vol. 47 (Marcel Dekker, New York, 1995).
2. I. N. Ross *et al*., J. Opt. Soc. Am. B **19**, 2945 (2002).
3. V. Bagnoud *et al*., Opt. Lett. **26**, 337 (2001).
4. T. Yu. Cherezova *et al*., Appl. Opt. **40**, 6026 (2001).
5. A. J. Campillo *et al*., Opt. Commun. **10**, 313 (1974).
6. G. Emiliani *et al*., Appl. Opt. **28**, 2832 (1989).
7. G. Giuliani, Y. K. Park, and R. L. Byer, Opt. Lett. **5**, 491 (1980).
8. G. Dubé, Opt. Commun. **12**, 344 (1974).
9. J. M. Auerbach and V. P. Karpenko, Appl. Opt. **33**, 3179 (1994).
10. B. M. Van Wonterghem *et al*., Appl. Opt. **36**, 4932 (1997).
11. G. H. Miller, E. I. Moses, and C. R. Wuest, Nucl. Fusion **44**, S228 (2004).
12. M. Henesian, Lawrence Livermore National Laboratory, Livermore, CA, private communication (2006).
13. J. H. Kelly, L. J. Waxer, V. Bagnoud, I. A. Begishev, J. Bromage, B. E. Kruschwitz, T. J. Kessler, S. J. Loucks, D. N. Maywar, R. L. McCrory, D. D. Meyerhofer, S. F. B. Morse, J. B. Oliver, A. L. Rigatti, A. W. Schmid, C. Stoeckl, S. Dalton, L. Folnsbee, M. J. Guardalben, R. Jungquist, J. Puth, M. J. Shoup III, D. Weiner, and J. D. Zuegel, J. Phys. IV France **133**, 75 (2006).
14. R. Ulichney, *Digital Halftoning* (MIT Press, Cambridge, MA, 1987).
15. J. Stoffel and J. Moreland, IEEE Trans. Commun. **29**, 1898 (1981).
16. R. W. Floyd and L. Steinberg, J. Soc. Inf. Disp. **17**, 75 (1976).
17. S. Weissbach and F. Wyrowski, Appl. Opt. **31**, 2518 (1992).
18. R. A. Ulichney, Proc. IEEE **76**, 56 (1988).
19. M. J. Madou, *Fundamentals of Microfabrication: The Science of Miniaturization* (CRC Press, Boca Raton, FL, 2002).